Received 21 April 2020; revised 2 July 2020; accepted 26 August 2020. Date of publication 31 August 2020; date of current version 8 December 2020.
The review of this article was arranged by Editor W. Grabinski.

Digital Object Identifier 10.1109/JEDS.2020.3020312

Advances in Compact Modeling of Organic Field-Effect Transistors

SUNGYEOP JUNG [1,2,3] (MEMBER, IEEE), YVAN BONNASSIEUX [4], GILLES HOROWITZ [4], SUNGJUNE JUNG [1,2] (MEMBER, IEEE), BENJAMIN IÑIGUEZ [5] (FELLOW, IEEE), AND CHANG-HYUN KIM [6] (SENIOR MEMBER, IEEE)

1 Future IT Innovation Laboratory, Pohang University of Science and Technology, Pohang 37673, South Korea
2 Department of Creative IT Engineering, Pohang University of Science and Technology, Pohang 37673, South Korea
3 Advanced Institute of Convergence Technology (AICT), Seoul National University, Suwon 16229, South Korea
4 LPICM, Ecole Polytechinque, CNRS, 91128 Palaiseau, France
5 DEEEA, Universitat Rovira i Virgili, 43007 Tarragona, Spain
6 Department of Electronic Engineering, Gachon University, Seongnam 13120, South Korea

CORRESPONDING AUTHOR: C.-H. KIM (e-mail: chang-hyun.kim@gachon.ac.kr)

This work was supported in part by the National Research Foundation of Korea (NRF) grant funded by the Korean Government (MSIT) under Grant NRF-2019R1C1C1003356, in part by Basic Science Research Program through the NRF funded by the Ministry of Education under Grant NRF-2018R1D1A1B07048877, in part by the IT Consilience Creative Program supervised by the Institute for Information and Communications Technology Promotion under Grant IITP-2019-2011-1-100783, and in part by the European Project H2020-MSCA-RISE-2014 (DOMINO) under Grant 645760.

ABSTRACT In this review, recent advances in compact modeling of organic field-effect transistors (OFETs) are presented. Despite the inherent strength for printed flexible electronics and the extremely aggressive research conducted over more than three decades, the OFET technology still seems to remain at a relatively low technological readiness level. Among various possible reasons for that, the lack of a standard compact model, which effectively bridges the device- and system-level development, is clearly one of the most critical issues. This article broadly discusses the essential requirements, up-to-date progresses, and imminent challenges for the OFET compact device modeling toward a universal, physically valid, and applicable description of this fast-developing technology.

INDEX TERMS Organic field-effect transistors (OFETs), compact modeling, device physics, circuit simulation, flexible and printed electronics.

I. INTRODUCTION

Since the first report by Tsumura *et al.* in 1986 [1], organic field-effect transistors (OFETs) have been considered as a key enabler for flexible and printed electronics [2]–[7]. The suitability of OFETs for such unconventional platforms is justified at the molecular level, where a weakly bound organic molecular solid (formed by van der Waals interaction) offers both low-energy-budget processing (e.g., direct printing or low-temperature sublimation) [8]–[10] and a low macroscopic young's modulus (ca. 1 GPa as compared to 130 GPa for Si) that translates into an excellent mechanical deformability [11]. Initially, relatively low charge-carrier mobility and environmental stability, which are otherwise associated with the same molecular nature (the weak electronic coupling and absence of covalent bonds between molecules), was a major problem of OFETs. Later, the tremendous efforts put into OFET materials synthesis and device engineering have brought truly impressive improvements on both fronts, making a range of air-stable, high-mobility OFETs available for use [12]–[15].

However, the commercialization of OFETs still seems to be slow, which we believe is partly due to the less emphasis placed on the circuit- and system-level investigation that is otherwise critically necessary for putting all these materials and devices into the context of viable technologies and potential real-world products. More specifically, we identify the lack of a standard compact model as one of the most important issues that need to be addressed, to generate a significant research momentum on circuit design and to motivate a more balanced and sustainable development chain for OFET technologies [16]–[18].

In this review, the principles, examples, and perspectives of OFET compact modeling are broadly introduced. Above all, we aim at providing sufficient basic information to both

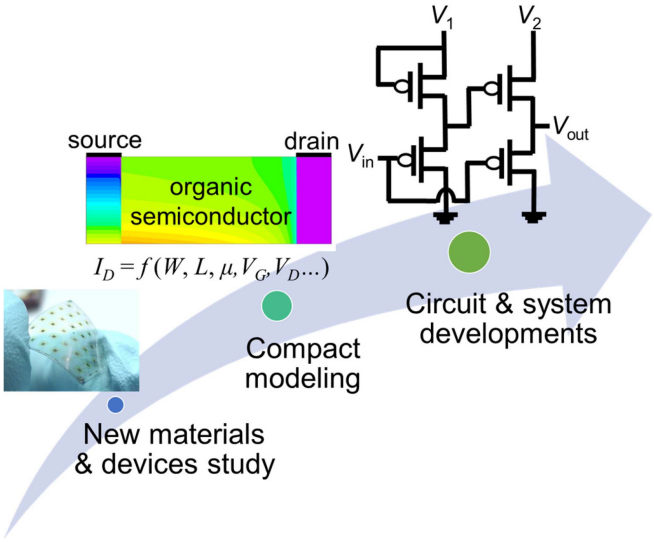

FIGURE 1. Conceptual representation of the general research and development steps toward industrial applications of a new electronic device technology.

the OFET and compact modeling communities, which will meaningfully bridge the currently significant gap between the two worlds. To fulfill that mission, many of our contents are intended to be selective rather than exhaustive. Nonetheless, a major strategy will be the clarification of the model development flow coupled with apparent advantages and limitations of current approaches. Following this introduction, Section II will address the general role of compact models in modern electronics research and clarify the fundamental requirements associated with the unique properties of OFETs. Sections III and IV constitute the body of this contribution, which will systematically re-visit reported DC and AC compact models, respectively. Section V will then suggest several aspects that can be a possible focus of future modeling. Finally, Section VI will close the paper with a concluding remark.

II. IMPORTANCE OF COMPACT MODELS

The compact modeling is an established topic in semiconductor research and development [17]. At the same time, it is still not so broadly concerned by the OFET community. Here, we briefly introduce the basic concepts of compact modeling and OFETs to further stimulate synergistic endeavors, which will also serve as a prerequisite to understanding reported models that will be highlighted in Sections III and IV.

A. COMPACT MODEL BASICS

A compact model of a specific device is a set of mathematical descriptions that establish the relationship between the terminal characteristics (e.g., drain current, capacitances) and a range of materials (e.g., carrier mobility, trap density), geometrical (e.g., channel dimensions, thicknesses), and operational parameters (e.g., temperature, voltages). Figure 1 illustrates the foremost importance of a compact model as an effective bridge between the device- and system-level outlooks. An emerging electronics technology generally starts with the discovery or elaboration of a new material or a new device architecture. This is often an experimental adventure, and involves a careful optimization of materials properties, processing, and device structures. The compact modeling refers to a broad range of activities aimed at creating and validating a new compact model. In many cases, the operating mechanism of a newly developed device is first analyzed through technology computer-aided design (TCAD) tools. These tools numerically solve relevant semiconductor physics equations (e.g., Fermi-Dirac, Poisson's, and continuity equations) and provide a comprehensive and quantitative relationship between terminal characteristics and a wide range of materials and device input parameters. However, such a numerical solution requires a substantial computational load, and therefore is not suitable for simulating a circuit that may integrate a large number of devices. A 'compact' modeling thus tries to simplify the tasks by capturing the most essential parts of the governing mechanisms into a relatively simple, and ideally analytical set of equations. Once a compact model for a new device is successfully prepared, we are ready to implement this model into a general-purpose circuit simulator (e.g., SPICE), and embark on a journey of system-level developments through the design, simulation, and prediction of functional circuits that contain this new device (and many other conventional ones). Now, we briefly discuss what is required for a good compact model.

A.1. DEVICE PHYSICS

A compact model should be supported by physical theories. While the simplification and fitting capability is a key to compact modeling, introducing too many empirical functions and parameters with no or weak physical meaning can eventually undermine the entire validity of the model.

A.2. SIMPLE EQUATIONS

As explained above, simpler expressions with a minimal number of parameters will benefit the process of solving for the currents or voltages inside an integrated circuit, by raising the chance of reaching a convergence over a short period of time. In the same sense, descriptions without numerical integration or derivation are of great interest.

A.3. WIDE APPLICABLE RANGE

As will be seen in Sections III and IV, the distinction between operation regimes is not so desirable, and ideally a single equation can be devised to cover as many regimes as possible. This will clearly reduce the number of equations and parameters to be included in a model library. If a model was validated through measuring a certain device, we should also care for the model's extended applicability to other devices (within the same family) with, for instance, different sizes and/or at varying temperatures.

One may notice that satisfying all these criteria will not be straightforward. This may partly explain why there are different possible models for the same device, as each model can place an emphasis on a different aspect of theories, implementation, or applicability.

B. SPECIFICITIES OF OFET MODELING

Organic materials are truly diverse by their nature. There already exist a large number of chemical moieties with known semiconducting properties, while the targeted synthesis of new molecules is an integral part of organic electronics research [19]–[22]. This constitutes the first and perhaps the most important consideration (and an obvious challenge) for the OFET compact modeling, as we do not want to develop a model valid for only one organic semiconductor. Also, even the same molecule can sometimes form vastly different solid-state film microstructures [23], [24], further challenging the universalism. Furthermore, the available options for materials processing and device structure are many (which can actually be an advantage in engineering) [25]–[27], so an OFET model that accounts for all the possible number of cases can be difficult to come up with. However, if this is something intrinsic to the technology, the efforts on developing an OFET model, which is intended to represent the whole range of materials and devices, should be oriented toward figuring out what are the unique and defining features of organic semiconductors and OFETs by comparison with other comparable technologies. At the material level, a low thermal carrier concentration and a low dielectric constant can be some of these characteristics, as these can significantly affect the electrostatics of the channel [28]–[30]. At the device level, the general absence of a doped contact region, two-dimensional current spreading, space-charge effects, chemical surface traps can be critical, which can in turn produce characteristics such as contact resistance (R_C), bulk conductivity, imperfect saturation, and threshold modulation.

III. SUMMARY OF RECENT DC MODELS

The recent progress in DC compact models has been made in describing the gate voltage dependence of mobility and R_C, in improving the transfer and output characteristics, and in expanding the operation regimes from the accumulation regime to the partial- and full-depletion regimes. In Sections III-A and III-B, the models focusing on the drift conduction are reviewed. These models are categorized into two groups according to how the gate dependence of mobility is incorporated. In Section III-C, models based the drift-diffusion theory are briefly explained.

A. APPROACH BASED ON KIM ET AL. [31] AND JUNG ET AL. [32]

The drift model for drain current is generally given by

$$I_{\text{above}} = W\mu Q_s(x)\frac{dV}{dx}, \tag{1}$$

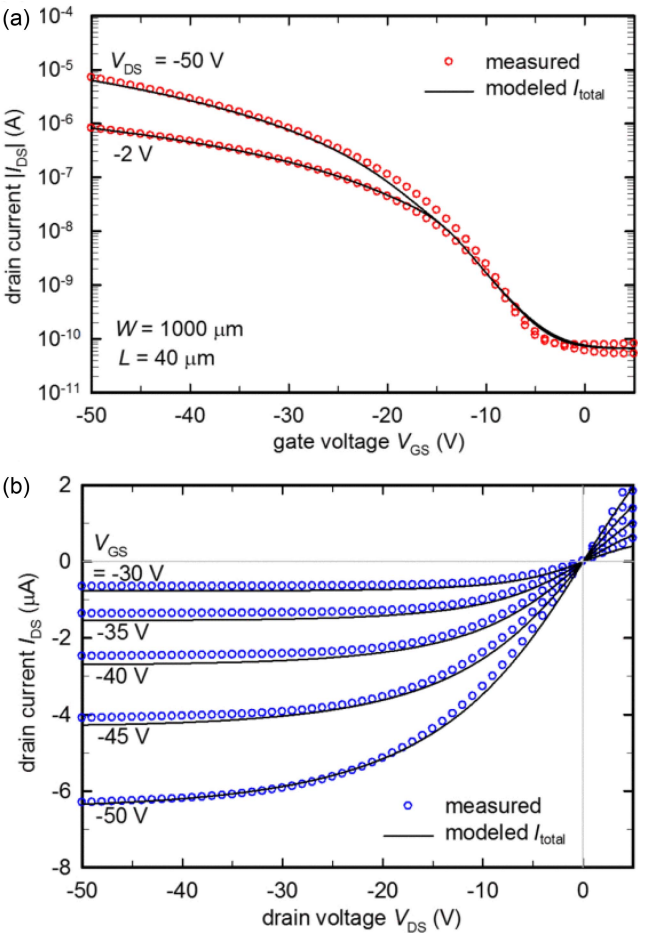

FIGURE 2. Comparison between the measured OFET characteristics and the model by Kim *et al.* [31] or (10) with a constant R_C ($A = 0$ and $R_C^{\infty} = R_C$). Reproduced from [31].

where W is the channel width, μ is the mobility, dV/dx is the electric field along the channel, and $Q_s(x)$ is the total charge per unit area induced by the gate voltage (V_{GS}) at a distance x from the source

$$Q_s(x) = C_i(-V_G + \psi_s(x)). \tag{2}$$

Here, C_i is the insulator capacitance per unit area and $\psi_s(x)$ is the surface potential.

By integrating (1) from source ($x = 0$ and $V = V_S = 0$) to drain ($x = L$ and $V = V_D$) upon assuming a linear surface potential along the channel, and with V_T as the threshold voltage,

$$\psi_s(x) = V(x) - V_T, \tag{3}$$

we get the drain current equation as

$$I_{\text{above}} = \frac{W}{L}\mu C_i\left[(V_{GS} - V_T)V_{DS} - \frac{V_{DS}^2}{2}\right]. \tag{4}$$

This basic model is derived assuming the constant mobility along the channel as well as no R_C. In addition, only the above-threshold regime is considered. During the

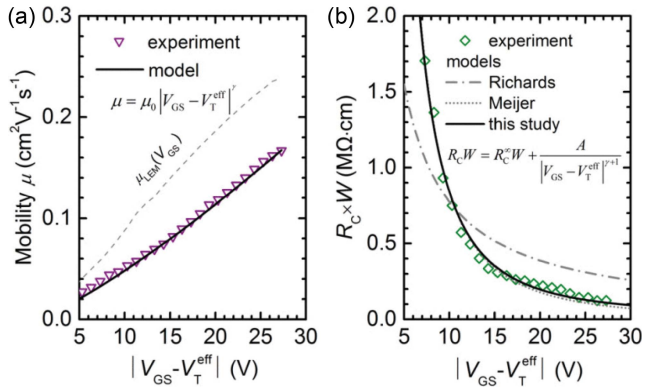

FIGURE 3. Comparison between the measured mobility and the power-law mobility model (5), and between the measured contact resistance and the asymptotic power-law model (8) by Jung *et al.* [32]. Reproduced from [32].

past decades, considerable improvements have been made to incorporate non-idealities and to describe all operation regimes.

For example, first, the V_{GS}-dependence of field-effect mobility is embraced by

$$\mu = \frac{\mu_0}{V_{aa}^{\gamma}}|V_{GS} - V_T|^{\gamma} \tag{5}$$

where μ_0 is the mobility prefactor, V_{aa} is the mobility enhancement voltage, and γ is the exponent of power-law mobility.

Second, V_{DSe} enables a smooth linear-to-saturation transition via the transition parameter m

$$V_{DSe} = V_{DS}\left[1 + \left(\frac{V_{DS}}{V_{Sat}}\right)^m\right]^{-\frac{1}{m}} \tag{6}$$

that approximated to the drain voltage (V_{DS}) when $V_{DS} \ll V_{sat}$ and to V_{sat} when $V_{DS} \gg V_{sat}$. Here, V_{sat} is the saturation voltage, $V_{sat} = \alpha_s(V_{GS} - V_T)$, and the saturation modulation parameter α_s modulates the onset voltage of saturation.

Third, an improved output asymptotic behavior is introduced by

$$I_{asym} = I_{sat}[1 + \lambda(V_{DS} - V_{sat})] \tag{7}$$

which provides solution to inaccurate overestimation of low-voltage output conductance [Fig. 2] [31].

Fourth, the gate dependence of R_C is introduced by Jung *et al.* [32] using an asymptotic power-law function [Fig. 3],

$$R_C = R_C^{\infty} + \frac{A/W}{\left|V_{GS} - V_T^{eff}\right|^{\gamma+1}}, \tag{8}$$

where R_C^{∞} is the contact resistance asymptote, A is the proportionality factor, and V_T^{eff} is the effective threshold voltage that contains the effect of V_{DS} ($V_T^{eff} = V_T + V_{DS}/2$) [33].

Considering the non-idealities (5)-(8), the complete above threshold drain current model is written as

$$I_{above} = \frac{\frac{W}{L}C_i\frac{\mu_0}{V_{aa}^{\gamma}}\left|V_{GS} - V_T^{eff}\right|^{\gamma+1}}{\left[1 + \frac{A\mu_0 C_i}{LV_{aa}^{\gamma}} + R_C^{\infty}\frac{W}{L}C_i\frac{\mu_0}{V_{aa}^{\gamma}}\left|V_{GS} - V_T^{eff}\right|^{\gamma+1}\right]} \times [1 + \lambda(|V_{DS}| - \alpha_s|V_{GS} - V_T|)] \times \frac{V_{DS}}{\left[1 + \left(\frac{V_{DS}}{\alpha_s|V_{GS}-V_T|}\right)^m\right]^{\frac{1}{m}}}, \tag{9}$$

which is an enhancement of the Unified Model and Extraction Method (UMEM) [34] to include symmetry around $V_{DS} = 0$ and a bias-dependent series resistance.

Finally, the total drain current I_{total} model is established [32]:

$$I_{total} = I_{above} \times \left[1 - \tanh\left[-\frac{(V_{GS} - V_T)}{(V_B - V_T)}\right]\right] + I_{sub} \times \left[1 + \tanh\left[-\frac{(V_{GS} - V_T)}{(V_B - V_T)}\right]\right] + I_{off}, \tag{10}$$

where V_B is the transition voltage, I_{off} is the off-current, and I_{sub} is the sub-threshold current

$$I_{sub} = I_{sub.0}\exp\left(-\frac{\ln 10}{S}(V_{GS} - V_T)\right). \tag{11}$$

Here, $I_{sub.0}$ is the drain current at threshold, and S is the sub-threshold swing.

The benefits of these models adopting the piecewise models interwoven by a transition function are 1) the simple and precise extraction procedures that can be used to determine all model parameters from the measured electrical characteristics, and 2) the ease of incorporation of additional features. With a single set of parameters, these models reproduced the measured off, subthreshold, linear, and saturation regimes [7], [32]. Recently, Zhao *et al.* [35], and Fan *et al.* [36] added the V_{GS} dependence of S and V_{DS} dependence of I_{off}. Other than these modifications, most aspects of the model are similar to those of [31] and [32].

B. APPROACH BASED ON CASTRO-CARRANZA ET AL. [37] AND MARINOV ET AL. [38]

The models by Castro-Carranza *et al.* [37] and Marinov *et al.* [38] are also drift-based models. However, they implement the V_{GS}-dependent mobility (5) in the drift current equation (1) before it is being integrated rather than in (4). As a result, the current equations are slightly different and are considered less empirical compared to the models in Section III-A.

By integrating (1), Castro-Carranza *et al.* derived the generic drain current model for the above-threshold regime:

$$I_{above} = \frac{W}{L}\frac{\mu_0}{V_{aa}^{\gamma}}C_i\left[\frac{(V_{GT} - V_{DS})^{2+\gamma} - (V_{GT})^{2+\gamma}}{2+\gamma}\right] \tag{12}$$

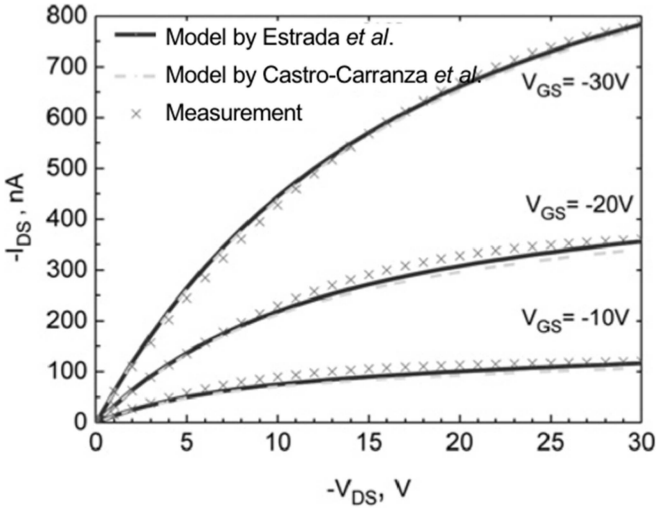

FIGURE 4. Comparison between the model by Estrada *et al.* [34] or (9) with constant R_C and without improved output asymptotic behavior, the model by Castro-Carranza *et al.* [37] or (13), and the measured output characteristics. Reproduced from [37].

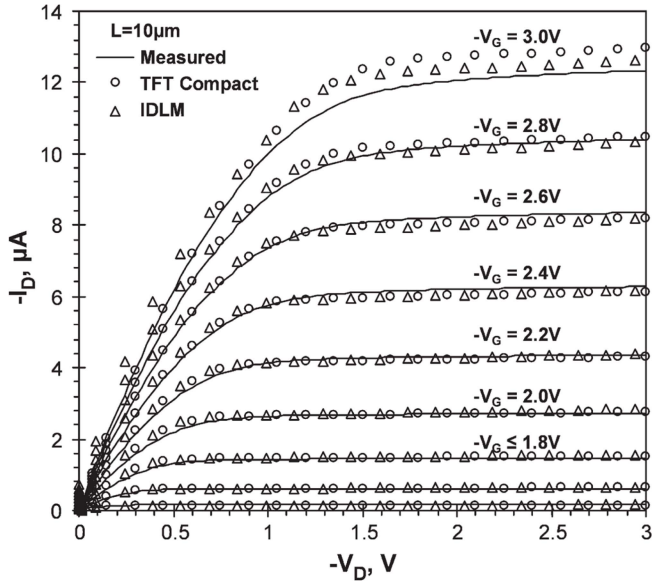

FIGURE 5. Comparison between the measured output characteristics and the model by Marinov *et al.* [38]: TFT compact indicates the implicit model (15). IDLM indicates the explicit injection-drift-limited model detailed in [38]. Reproduced from [38].

By replacing V_{DS} in (12) with V_{DSe} of (6) and introducing the output asymptotic behavior, the complete above threshold drain current model is written as [Fig. 4]

$$I_D = \frac{W}{L}\frac{\mu_0}{V_{aa}^{\gamma}}C_i\left[(V_{GT} - V_{DSe})^{2+\gamma} - (V_{GT})^{2+\gamma}\right] \times \frac{(1+\lambda V_{DS})}{2+\gamma} \tag{13}$$

The UMEM [34] or (9) can be obtained from the linearization of (13) around $V_{DS} = 0$. The parameters of this non-linear model are otherwise the same as the UMEM.

Similarly, Marinov *et al.* [38] derived the drain current equation for the accumulation regime as

$$I_{above} = \frac{W}{L}\frac{\mu_0}{V_{aa}^{\gamma}}C_i \times \left[\frac{(V_G - V_T - V_S)^{2+\gamma} - (V_G - V_T - V_D)^{2+\gamma}}{2+\gamma}\right] \tag{14}$$

This model, in its generic form, does not consider the sub-threshold regime similar to the model by Castro-Carranza *et al.* Therefore, the sub-threshold regime is included by an asymptotic interpolation function,

$$I_D = \frac{W}{L}\frac{\mu_0}{V_{aa}^{\gamma}}C_i \times \left[\frac{[f(V_G - V_T - V_S)]^{2+\gamma} - [f(V_G - V_T - V_D)]^{2+\gamma}}{2+\gamma}\right] \tag{15}$$

where, with either $V = V_D$ or $V = V_S$, the function $f(V_G, V)$ can be regarded as effective voltage overdrive V_{EODR} given by

$$\begin{aligned} V_{EODR}(V) &= f(V_G, V) \\ &= V_{SS}\ln\left[1 + \exp\left(\frac{V_G - V_T - V}{V_{SS}}\right)\right] \\ &\approx \begin{cases} V_{SS}\exp\left(\frac{V_G - V_T - V}{V_{SS}}\right), & \text{when } V_G - V_T - V < V_{SS} \\ V_G - V_T - V, & \text{when } V_G - V_T - V > V_{SS}. \end{cases} \end{aligned} \tag{16}$$

Here, V_{SS} is the parameter that is related to the steepness of the sub-threshold characteristics of the thin-film transistor (TFT).

This model also considers the channel length modulation in a similar approach as (10), yielding

$$I_D = \frac{W}{L}\frac{\mu_0}{V_{aa}^{\gamma}}C_i\left[(V_G - V_T - V_S)^{2+\gamma} - (V_G - V_T - V_D)^{2+\gamma}\right]\frac{(1+\lambda V_{DS})}{2+\gamma}. \tag{17}$$

In addition, this model incorporates the voltage drop V_C across the contacts assuming a functional model of the carrier injection as $V_C = f_C(I_D) = V_C(I_D)$. Then the generic model (14) becomes [Fig. 5]

$$I_D = \frac{W}{L}\frac{\mu_0}{V_{aa}^{\gamma}}C_i \times \left[\frac{(V_G - V_T - V_C(I_D))^{2+\gamma} - (V_G - V_T - V_D)^{2+\gamma}}{2+\gamma}\right]. \tag{18}$$

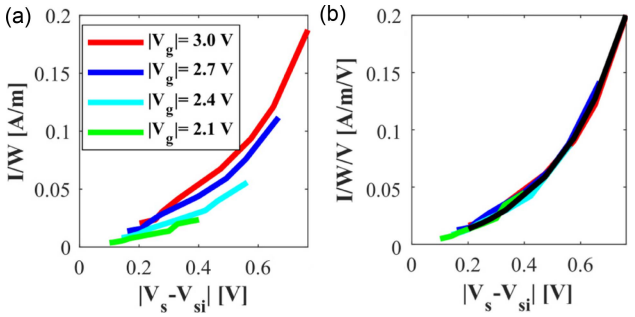

FIGURE 6. Width-normalized current-voltage characteristics of the source contact (a) for V_{GS} = 2.1, 2.4, 2.7 and 3 V, and (b) normalized to the gate-field-accumulated charge density by dividing by $(V_{Si} - V_G + V_T)^{0.8}$. Reproduced from [39].

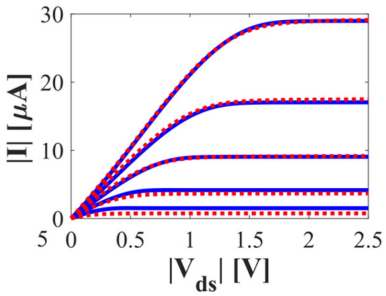

FIGURE 7. Comparison between the measured (red dotted line) output characteristics of a short channel OFET and the model (blue solid line) by Elsaegh *et al.* [39] or (17)-(21): L_{ch} = 4 μm, W_{ch} = 200 μm. Fitting of a long channel OFET with L_{ch} = 100 μm, W_{ch} = 200 μm is also available. Reproduced from [39].

This feature is advantageous compared to the model by Castro-Carranza *et al.* However, the model possesses a weakness that most TFT compact models have in common: the drain current is an implicit function of R_C.

Recently, Elsaegh *et al.* [39] modified the model by Marinov *et al.* [38] and derived an explicit function for the contact voltage drop. This model assumes that the intrinsic saturation-regime drain current can be written as

$$I_{sat} = \frac{1}{2}\frac{W_{eq}}{L_{ch}}\mu_0 C_i (V_{Si} - V_G - V_T)^2, \tag{19}$$

where $W_{eq} = W_{ch} + W_{fringe}$ is the equivalent width that is equal to the channel and fringe width, V_{Si} is the potential in the channel at the location closest to the source side to which contact voltage drop V_C occurs. In addition, the model assumes that the extrinsic saturation-regime drain current including the source contact effect can be written as

$$I_{sat} = \frac{1}{2}\frac{W_{eq}}{L_{ch} + L_{ex}}\mu_0 C_i (V_{Si} - V_G + V_T)^2, \tag{20}$$

where $L_{ch} + L_{ex}$ is the equivalent channel length L_{eq}. Solving (19) and (20) with V_S grounded, V_{Si} could be derived as

$$V_{Si} = (V_T - V_G)\left(\sqrt{\frac{L_{ch}}{L_{eq}}} - 1\right), \tag{21}$$

Then, the authors showed that the measured drain current normalized by the effective width and the effective voltage overdrive $(V_{Si} - V_G + V_T)^{0.8}$ with respect to the source contact potential [Fig. 6] could be fit to an exponential function for the reverse-biased Schottky-diode model (black line).

Finally, the compact model represents the drain current as a set of equations:

$$I_D = \frac{W_{eq}}{2L_{eq}}\mu_0 C_i \left[f(V_{Si}, V_G)^2 - f(V_{Di}, V_G)^2\right] \times (1 + \lambda(V_{Di} - V_{Si})). \tag{22}$$

$$I_D = tJ_{os}W_{eq}\left(e^{\frac{V_S - V_{Si}}{\eta_s V_{th}}} - 1\right)(V_{Si} - V_G - V_T)^{P_{snorm}} \tag{23}$$

$$I_D = tJ_{od}W_{eq}\left(e^{\frac{V_{Di} - V_D}{\eta_s V_{th}}} - 1\right)(V_{Di} - V_G - V_T)^{P_{dnorm}} \tag{24}$$

where the first equation corresponds to the intrinsic model, and the second and the third equation correspond to the source contact current model and the drain contact current model based on a reversed-biased Schottky-diode model. Here, t is the effective injection length, J_{os} is the current density underneath the gate-source overlap, J_{od} is the same underneath the gate-drain overlap, the gate-drain overlap, V_{th} is the thermal voltage, η_s is the nonideality factor, P_{snorm} is the charge-normalization power factor at the source contact, and P_{dnorm} is the same at the drain contact. In the case of inverted staggered OFETs, t is equal to the overlap length L_{ov}. On the other hand, t is equal to the thickness of the source/drain contacts. This model shows a good agreement with the measured transistor characteristics [Fig. 7].

Although the generic models by Castro-Carranza *et al.* and Marinov *et al.* are meant to cover the sub-threshold regime as well as the above-threshold regime, the approaches using the linear-to-saturation transition voltage V_{DSe} and the effective voltage overdrive V_{EODR} are empirical. However, since the terminal charge models are available in an analytical form, these models establish an important foundation for quasi-static AC models for OFETs as will be discussed later.

C. DRIFT-DIFFUSION APPROACH

Recently, there has been an alternative approach to including both sub-threshold and above-threshold regimes in the drain current model by a direct solution of drift-diffusion equation [40], [41]:

$$I_D = W\mu\left(Q_s(x)\frac{dV}{dx} + \frac{k_B T}{q}\frac{dQ_s(x)}{dx}\right). \tag{25}$$

The approach by Colalongo [40], which includes variable range hopping, requires numerical resolution of a non-linear equation. The approach by Hain *et al.* [41] leads to an analytical closed-form model based on the Lambert's W-function. In this model, charges in shallow traps are treated as quasi-free carriers transported by the drift-diffusion mechanism, while the hopping transport is taken into account by an effective power-law mobility. The Schottky barrier effect (non-linear injection) is incorporated by considering a non-linear resistance in series to R_C, and by including the

total resistance in the effective mobility as a second-order correction [42]. Compared to the models in Sections III-A and III-B, the method of solving the drift-diffusion equation supports the sub-threshold regime in a more physical rigorousness way. On the other hand, numerical approaches may compromise the ease of parameter extraction. Also, the approximations used upon the solution and derivation must be examined carefully.

IV. SUMMARY OF RECENT AC MODELS

Previous AC models for OFET adopt the quasi-static approach from MOSFETs. The quasi-static assumption is that the rate of change of the biasing is slow enough, so that at any time and position in the channel the charges are identical to those under DC biasing [43], i.e., it does not consider frequency effects. The first aim of recent AC model for OFETs has been to encompass all operation regimes [37], [44]. The second aim was to describe the frequency dependence of $C-V$ characteristics [45] and experimental validation of such behavior [46].

A. APPROACH BASED ON CASTRO-CARRANZA ET AL. [37]

The model by Castro-Carranza *et al.* [37] is a quasi-static and continuous model in the entire above-threshold regime for the complete nine nonreciprocal capacitances:

$$C_{\mathrm{ij}} = -\frac{\partial Q_{\mathrm{i}}}{\partial V_{\mathrm{j}}} \quad \mathrm{i} \neq \mathrm{j} \tag{26}$$

$$C_{\mathrm{ij}} = \frac{\partial Q_{\mathrm{i}}}{\partial V_{\mathrm{j}}} \quad \mathrm{i} = \mathrm{j} \tag{27}$$

where i and j refers to any of the three electrodes of the OFETs, i.e., gate G, drain D, and source S.

This model includes intrinsic capacitance and extrinsic capacitances caused by the physical proximity of the gate and the source or drain. The gate-source and gate-drain overlap capacitance is calculated as

$$C_{\mathrm{OV}} = WL_{\mathrm{OV}}C_{\mathrm{i}} \tag{28}$$

The total capacitances are written as

$$C_{\mathrm{GG}} = WLC_{\mathrm{i}}(2+\gamma)\left[1 - \frac{(2+\gamma)A_1A_3}{(3+\gamma)A_2^2}\right] + 2C_{\mathrm{OV}} \tag{29}$$

$$C_{\mathrm{GD}} = \frac{WLC_{\mathrm{i}}(2+\gamma)}{A_2} \times \left[V_{\mathrm{GT}}^{2+\gamma} - \frac{(2+\gamma)(V_{\mathrm{GT}} - V_{\mathrm{DSe}})^{1+\gamma}A_3}{(3+\gamma)A_2}\right] + C_{\mathrm{OV}} \tag{30}$$

$$C_{\mathrm{DD}} = \frac{WLC_{\mathrm{i}}(2+\gamma)}{A_2^2} \times \left[(V_{\mathrm{GT}} - V_{\mathrm{DSe}})^{4+2\gamma} + (4+2\gamma) \times (V_{\mathrm{GT}} - V_{\mathrm{DSe}})^{1+\gamma}N_{\mathrm{D1}} - N_{\mathrm{D2}}\right] + C_{\mathrm{OV}} \tag{31}$$

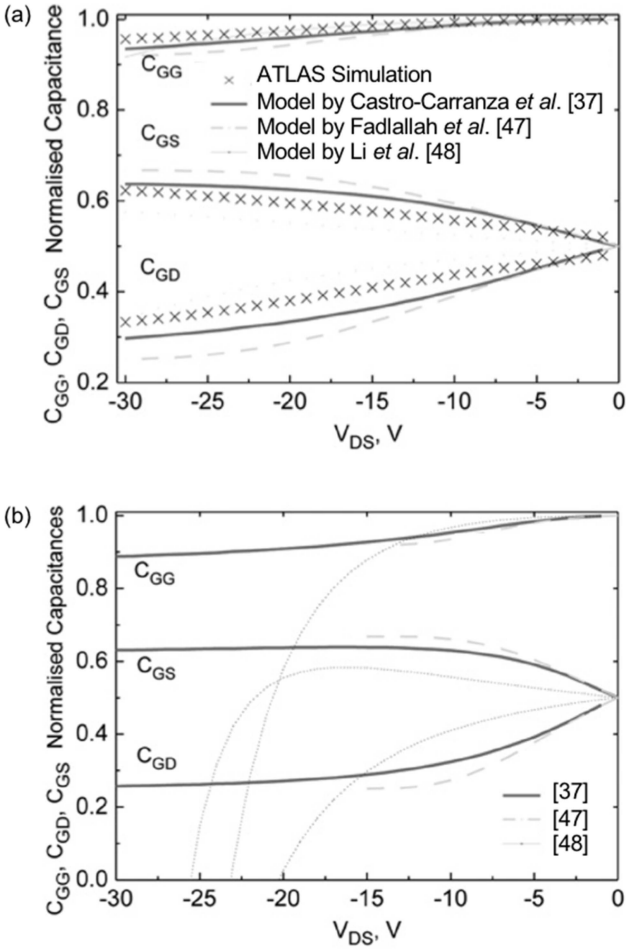

FIGURE 8. Model by Castro-Carranza *et al.* [37]. Comparison of C_{GG}, C_{GD}, and C_{GS} in (a) linear regime ($V_{GS} = -30$ V) and (b) saturation regime $V_{GS} = -10$ V. Reproduced from [37].

$$C_{\mathrm{DG}} = \frac{WLC_{\mathrm{i}}(2+\gamma)}{A_2^2} \times \left[D - \frac{(4+2\gamma)N_{\mathrm{DG}}A_1}{A_2} - \frac{(2+\gamma)V_{\mathrm{GT}}^{1+\gamma}A_3}{(3+\gamma)} - V_{\mathrm{GT}}^{2+\gamma}A_2\right] + C_{\mathrm{OV}} \tag{32}$$

as a function of the gate-source overdrive voltage $V_{\mathrm{GTS}} = V_{\mathrm{GS}} - V_{\mathrm{T}}$ and the effective drain-source voltage V_{DSe} (6), where A_1, A_2, A_3,

$$A_1 = (V_{\mathrm{GT}} - V_{\mathrm{DSe}})^{1+\gamma} - V_{\mathrm{GT}}^{1+\gamma} \tag{33}$$

$$A_2 = (V_{\mathrm{GT}} - V_{\mathrm{DSe}})^{2+\gamma} - V_{\mathrm{GT}}^{2+\gamma} \tag{34}$$

$$A_3 = (V_{\mathrm{GT}} - V_{\mathrm{DSe}})^{3+\gamma} - V_{\mathrm{GT}}^{3+\gamma} \tag{35}$$

and N_{D1}, N_{D2}, N_{DG}, B, D,

$$N_{\mathrm{D1}} = \left[\frac{V_{\mathrm{GT}}^{2+\gamma}A_3}{(3+\gamma)A_2} - \frac{\mathrm{B}}{(5+2\gamma)A_2}\right] \tag{36}$$

$$N_{\mathrm{D2}} = V_{\mathrm{GT}}^{2+\gamma}(V_{\mathrm{GT}} - V_{\mathrm{DSe}})^{2+\gamma} \tag{37}$$

$$N_{DG} = \left[\frac{B}{(5+2\gamma)} - \frac{V_{GT}^{2+\gamma}A_3}{(3+\gamma)}\right] \tag{38}$$

$$B = (V_{GT} - V_{DSe})^{5+2\gamma} - V_{GT}^{5+2\gamma} \tag{39}$$

$$D = (V_{GT} - V_{DSe})^{4+2\gamma} - V_{GT}^{4+2\gamma}. \tag{40}$$

Compared to the previously reported models [47], [48], this model abides by the charge conservation rule by which other 5 capacitances C_{GS}, C_{DS}, C_{SG}, C_{SD} and C_{SS} could be determined completely.

By introducing V_{DSe} to this model, the authors achieved a smooth transition from linear to saturation regime. Thereby, this model provides better fit to simulated C-V characteristics [Fig. 8] compared to [47], [48]. Furthermore, this model is also under the framework of the UMEM [34]. Therefore, central parameters, such as V_T and γ, are common to the DC model. Other fitting parameters, such as m^* that adjust knee of the output I-V characteristics and β that adjust the onset of the saturation, are also common. This implies that the quantitative analysis can be done on these parameters using the AC characteristics of the device.

B. APPROACH BASED ON MARINOV AND DEEN [44]

The model by Marinov and Deen [44] is also a quasi-static and continuous model in the above threshold regime for the complete nine reciprocal capacitances.

$$C_{GG} = WLC_i\left[N_G\left\{1 + (1-\xi)\frac{(2+\gamma)\xi^{1+\gamma}}{1-\xi^{2+\gamma}}\right\} - (1-\xi)\frac{(2+\gamma)\xi^{2+\gamma}}{1-\xi^{2+\gamma}}\right], \tag{41}$$

$$C_{GD} = WLC_i\left[N_G\left\{\frac{(2+\gamma)\xi^{1+\gamma}}{1-\xi^{2+\gamma}}\right\} - \frac{(2+\gamma)\xi^{2+\gamma}}{1-\xi^{2+\gamma}}\right], \tag{42}$$

$$C_{DD} = WLC_i\left[N_D\left\{1 + 2(1-\gamma)\frac{(2+\gamma)\xi^{1+\gamma}}{1-\xi^{2+\gamma}}\right\} - (1-\gamma)\frac{(2+\gamma)\xi^{2+\gamma}}{1-\xi^{2+\gamma}}\right], \tag{43}$$

$$C_{DG} = WLC_i\left[N_D\left\{2\frac{(2+\gamma)\xi^{1+\gamma}}{1-\xi^{2+\gamma}}\right\} - \frac{(2+\gamma)\xi^{2+\gamma}}{1-\xi^{2+\gamma}}\right], \tag{44}$$

as a function of the non-saturation factor ξ,

$$\xi = \frac{V_{GTD}}{V_{GTS}} \approx \frac{V_G - V_T - V_D}{V_G - V_T - V_S}, \tag{45}$$

where V_{GTD} and V_{GTS} are the effective gate-drain and gate-source overdrive voltages with the voltage parameter $V_{SS} \approx 0.43(2+\gamma)SS$,

$$V_{GTD/GTS} = V_{SS}\left[1 + \exp\left(\frac{V_G - V_T - V_{D/S}}{V_{SS}}\right)\right]. \tag{46}$$

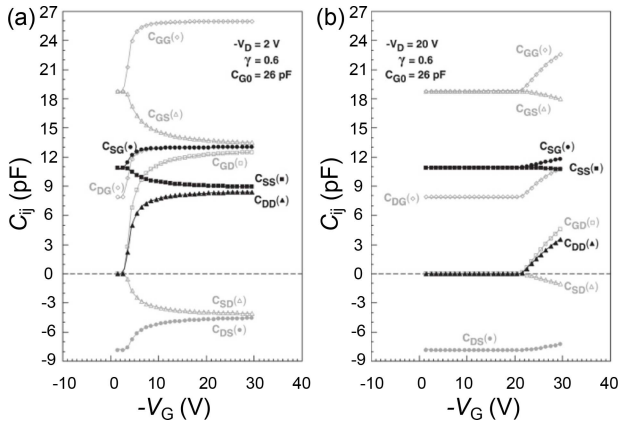

FIGURE 9. Model by Marinov and Deen [44]. Comparison of C_{GG}, C_{GD}, and C_{GS} in (a) linear regime ($V_{DS} = -2$ V) and (b) saturation regime $V_{DS} = -20$ V. Reproduced from [44].

N_G, N_D, and N_S are the normalized terminal charges:

$$N_G = \left(\frac{2+\gamma}{3+\gamma}\right)\left(\frac{1-\xi^{3+\gamma}}{1-\xi^{2+\gamma}}\right), \tag{47}$$

$$N_D = \left(\frac{2+\gamma}{3+\gamma}\right)\frac{\frac{2+\gamma}{5+2\gamma} - \xi^{3+\gamma} + \frac{3+\gamma}{5+2\gamma}\xi^{5+2\gamma}}{\left(1-\xi^{2+\gamma}\right)^2}, \tag{48}$$

$$N_S = \left(\frac{2+\gamma}{3+\gamma}\right)\frac{\frac{3+\gamma}{5+2\gamma} - \xi^{2+\gamma} + \frac{2+\gamma}{5+2\gamma}\xi^{5+2\gamma}}{\left(1-\xi^{2+\gamma}\right)^2} = N_G - N_D. \tag{49}$$

This describes the capacitances well for both linear and saturation regimes [Fig. 9].

It is a major contribution that the authors provided the circuit simulation results of a ring oscillator as well as Verilog-AMS translation of this compact model. The authors emphasized that the numerical errors are critical in practice and provided with a solution. For example, errors that occurs when subtracting large and similar values of V_{GTD} and V_{GTS} as well as dividing by zero when $V_D = V_S$ could be resolved by normalization of terminal charges in (47)-(48) and by addition of proportional parts in the numerators and denominators.

Despite the significant merits of this model, partial- and full-depletion regimes are not dealt as in the previous model of Castro-Carranza *et al.*

C. APPROACH BASED ON CASTRO-CARRANZA ET AL. [45]

Castro-Carranza *et al.* extended the quasi-static model from the accumulation regime (i.e., above-threshold regime) to the partial- and full-depletion regimes (i.e., sub-threshold and off regimes) and included non-quasi-static effects, i.e., the frequency dependence of $C-V$ characteristics [45]. The authors also provided a comparison between $C-V$ characteristics from the compact model and the measurement.

First, this model includes the equivalent capacitance C_{eq} which considers the depletion capacitance C_D of the organic

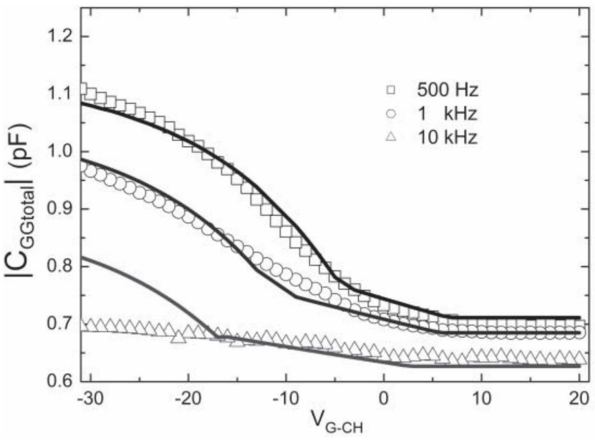

FIGURE 10. Comparison between the measured (symbols) $C-V$ characteristics of the PMMA/PCDTBT OFET and the model (solid lines) by Castro-Carranza *et al.* [45] at different frequencies. Reproduced from [45].

semiconductor in series with the gate insulator capacitance $C_{\rm i}$ in deep sub-threshold regime:

$$C_{\rm eq} = \begin{cases} \frac{C_{\rm D}C_{\rm i}}{C_{\rm D}+C_{\rm i}}, & if\ V_{\rm GS} > V_{\rm T} \\ C_{\rm i}, & if\ V_{\rm GS} > V_{\rm T} \end{cases} \tag{50}$$

where $C_{\rm D} = \varepsilon_{\rm s}LW/W_{\rm D}$, $\varepsilon_{\rm s}$ is the permittivity of the semiconductor layer, L is the channel length of the device, W is the channel width of the device, and $W_{\rm D}$ is the depletion width

$$W_{\rm D} = -\frac{\varepsilon_{\rm s}}{C_{\rm i}} + \sqrt{\frac{\varepsilon_{\rm s}^2}{C_{\rm i}^2} + \frac{2\varepsilon_{\rm s}|V_{\rm GS}-V_{\rm T}|}{qN_{\rm B}}} \tag{51}$$

where $N_{\rm B}$ is the semiconductor concentration which is $\sim 10^{14}$ cm^{-3} in non-intentionally doped molecular semiconductors and upto 10^{17} cm^{-3} in polymer semiconductors.

Then, the total capacitance is formulated by the sum of the capacitances in the accumulation regime $C_{\rm GG}$ and in the depletion regime $C_{\rm eq}$ joint by a tanh function:

$$C_{\rm GGtotal} = |C_{\rm eq}|\frac{1-\tanh\beta}{2} + |C_{\rm GG}|\frac{1-\tanh\beta}{2} \tag{52}$$

where $\beta = (V_{\rm GS}+\Delta_{\rm T})Q_2$, and $\Delta_{\rm T}$ is the shift in the threshold voltage of the $C-V$ characteristics at different frequencies, and Q_2 is a transition parameter.

Second, this model considers the frequency dependence of the accumulation capacitance to the applied ac signal. An empirical formula by Cole and Cole describes the variation of the dielectric constant,

$$\varepsilon_{\rm i} = \varepsilon_{\rm i\infty} + \frac{\varepsilon_{\rm i0}-\varepsilon_{\rm i\infty}}{1+\left(\frac{\omega}{2\pi\eta}\right)^{1.78p}} \tag{53}$$

where $\varepsilon_{\rm i0}$ and $\varepsilon_{\rm i\infty}$ are the permittivity at very low and very high frequencies, respectively, and ω is the angular ac frequency. For the dielectric constant of PMMA, the fitting parameters were $\eta = 207$ and $p = 0.22$. By putting (53) into (52), the authors formulated the frequency-dependent

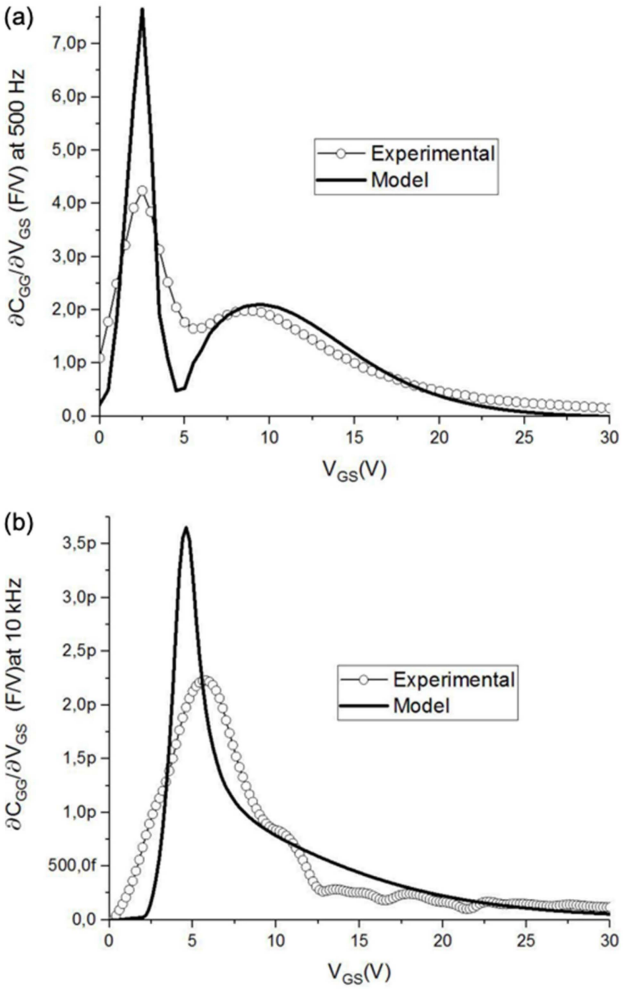

FIGURE 11. Comparison between the measured (symbols) first derivative of $C_{\rm GGtotal}$ versus $V_{\rm GS}$ and the model (solid lines) by Castro-Carranza *et al.* [45] at (a) 500 Hz and (b) 10 kHz. Reproduced from [46].

capacitance. In [46], the transition between the subthreshold and the above threshold regime was smoothened by a continuous interpolation function as an effective gate voltage overdrive.

The model accurately describes all gate bias domain and all operating regimes at low and medium frequencies [Fig. 10]. This model is shown valid for typical OFETs upto 10 kHz. At high frequencies, non-quasi-static effects are significant [46]. These effects are experimentally observed in the first derivative of $C_{\rm GGtotal}$ versus $V_{\rm GS}$ plot, which manifest in a more complex manner in accumulation regime compared to the depletion regime [Fig. 11]. Modeling these features by means of other physical models beyond the frequency dependence of the dielectric constant of the gate insulator is required. In [49], an equivalent circuit model was presented to account for all non-quasi-static effects in OFET capacitors.

There are also other emerging concepts and approaches for AC modeling. For instance, Leise *et al.* [50] proposed an analytical closed-form model in the Lambert's W-function for

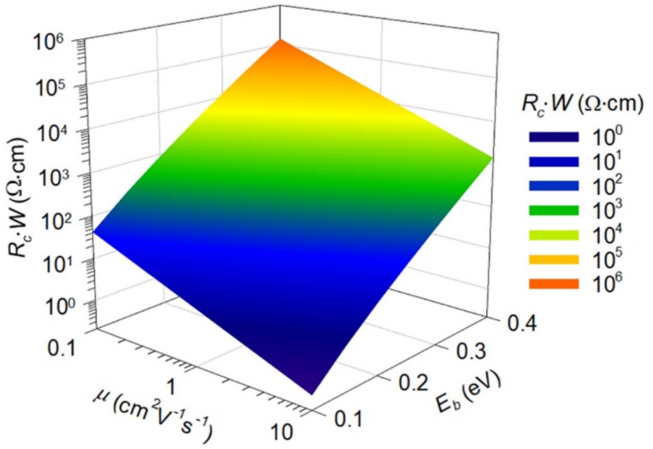

FIGURE 12. **Prediction made by a physical contact resistance model. Reproduced from [58].**

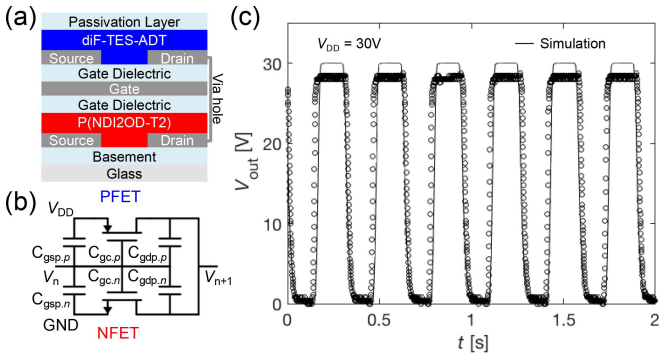

FIGURE 13. **(a) Cross-sectional illustration and (b) circuit diagram with multi-component overlap capacitances of the printed 3-D organic complementary inverter, and (c) measured and simulated transient output voltage of an 11-stage ring oscillator. Reproduced from [64].**

the quasi-mobile charges [41]. This was further extended to account for the multi-finger contacts and fringing effects by introducing the effective channel and gate widths [51]. The model was in good agreement with experimental data in both linear and saturation regimes under quasi-static operation.

V. KEY REQUIREMENTS FOR FUTURE DEVELOPMENTS

The two previous sections clearly demonstrated the remarkable progresses made for OFET compact modeling. However, there are a number of remaining challenges, for further improving both the theoretical robustness and practical applicability of the models. Here, we critically assess some of the representative issues that can be a direct focus of future modeling work.

A. PHYSICAL MODEL FOR MOBILITY AND CONTACT RESISTANCE

Most of the published models take the power-law mobility of the form similar to (5). This offers a capability of capturing the widely observed gate-enhancement of mobility into a simple, fully analytical expression [52]. Strictly speaking, such a mobility is only exact for the charge transport mediated by an exponential density of states (DOS). Therefore, its accuracy can be insufficient for disordered semiconductors with a Gaussian DOS [53], [54]. Ideally, a universal function that can support any possible DOS and transport scenarios, for instance through an embedded tuning parameter, is worth seeking, but this may not be simple to derive considering the difficulty in extracting an analytical formula out of a non-exponential DOS [55].

The R_C is another important characteristic of OFETs [56]. As its impact on device performance is broadly accepted [14], incorporating an improved physical R_C model into a compact modeling framework becomes a timely strategy. Recently, Kim and Horowitz published a fully analytical R_C model [Fig. 12] that illustrates its functional dependence on both mobility (μ) and charge-injection barrier (E_b) [57], which is later extended to projecting the theoretical frequency limit of OFETs [58]. The advantage of such an approach is to be able to correlate a major macroscopic feature to an interface injection phenomenon. This or other related functions can later be incorporated into both DC and AC equations, which can also possibly include a secondary correlation of E_b with several existing parameters other than R_C.

B. DEFINING THRESHOLD VOLTAGE

The V_T is a well-established concept in classical field-effect transistors. In contrast, even its existence and origins are still highly debated in OFETs. As a result, some compact models choose to include V_T as a stand-alone fitting parameter, yet others indirectly describe the channel formation. However, a functional breaking down of V_T and its incorporation into an OFET model is highly desirable, as it will allow for a simple calculation of the charge density based on its proportionality to the gate-overdrive voltage. In this regard, fundamental research on understanding V_T and its application to compact models will remain as a valuable research subject. For instance, previous studies suggested influential phenomena for an OFET V_T as a mobility enhancement [59], space-charge effects [60], E_b [33], and the transistor layout [61]. We also note that the possible variety of V_T extraction methods is not much addressed in OFETs [62], which is otherwise critical to both the precise definition and modeling application of V_T [63].

C. DEDICATED EFFORTS ON PRINTED ELECTRONICS

Printing is a low-cost route to fabricating OFET circuits, which is believed to be one of the most promising techniques that fully leverage the unique properties of organic electronic materials [26]. Therefore, the future OFET modeling can more directly reflect the specificities of printing process and printed devices. For instance, the minimum feature size of printed device layers is generally larger than that of photographically prepared ones. This can imply a considerable shift in the range of focus in a device model. For instance,

channel dimensions and overlap capacitances can be significantly high in printed transistors. Recently, Jung *et al.* reported on the modeling-driven design and simulation of printed organic circuits, directly addressing such critical issues as shown in Fig. 13 [64]. The printing-based fabrication has also pushed the development of three-dimensionally integrated circuit layouts [10], [65], [66] which is a smart way to overcome the limited transistor-per-area density. For such a new stream of technology, an advanced compact model can seek the systematic ways to incorporate the potential vertical interaction between transistors and expected impacts of multi-component overlap capacitances.

VI. CONCLUSION

The OFET technology stands at the crossroads of development. Despite the dramatic progresses made for device performances, the competition with other technologies is increasing, making the bright future of OFETs questionable. This review tried to merge and re-direct the accumulated scientific knowledges on various aspects of OFETs in envisioning their successful commercialization. Although there are numerous challenges to get there, we believe that transforming the well-established, but mostly scattered understanding and theories on transport, morphology, contacts, and interfaces into a unified compact model can be a key milestone. It is our expectation that the systematic overview and critical discussions provided in this article will promote further investigations on either refining the reported approaches toward more applicable and reliable ones or creating entirely new approaches. In any case, the organic circuit development will be substantially accelerated when a fully validated, generally accepted model becomes available in a wide range of design and engineering activities. This may in turn cast a fresh new momentum, on reviving or even boosting the potential of OFETs in a future characterized by flexible, mobile, easy-to-fabricate, and functionally tunable electronics.

REFERENCES

[1] A. Tsumura, H. Koezuka, and T. Ando, "Macromolecular electronic device: Field-effect transistor with a polythiophene thin film," *Appl. Phys. Lett.*, vol. 49, no. 18, pp. 1210–1212, Nov. 1986.
[2] G. Horowitz, "Organic field-effect transistors," *Adv. Mater.*, vol. 10, no. 5, pp. 365–377, Mar. 1998.
[3] G. Horowitz, "Organic thin film transistors: From theory to real devices," *J. Mater. Res.*, vol. 19, no. 7, pp. 1946–1962, Jul. 2004.
[4] D. Braga and G. Horowitz, "High-performance organic field-effect transistors," *Adv. Mater.*, vol. 21, nos. 14–15, pp. 1473–1486, Apr. 2009.
[5] H. Klauk, "Organic thin-film transistors," *Chem. Soc. Rev.*, vol. 39, no. 7, pp. 2643–2666, Jul. 2010.
[6] G. Gelinck, P. Heremans, K. Nomoto, and T. D. Anthopoulos, "Organic transistors in optical displays and microelectronic applications," *Adv. Mater.*, vol. 22, no. 34, pp. 3778–3798, Sep. 2010.
[7] C.-H. Kim, Y. Bonnassieux, and G. Horowitz, "Compact DC modeling of organic field-effect transistors: Review and perspectives," *IEEE Trans. Electron Devices*, vol. 61, no. 2, pp. 278–287, Feb. 2014.
[8] I. Kymissis, *Organic Field Effect Transistors: Theory, Fabrication and Characterization*. New York, NY, USA: Springer, 2008.
[9] M. M. Hussain and N. El-Atab, *Handbook of Flexible and Stretchable Electronics*. Boca Raton, FL, USA: CRC Press, 2019.
[10] J. Kwon, Y. Takeda, R. Shiwaku, S. Tokito, K. Cho, and S. Jung, "Three-dimensional monolithic integration in flexible printed organic transistors," *Nat. Commun.*, vol. 10, p. 54, Jan. 2019.
[11] T. Someya, Z. Bao, and G. G. Malliaras, "The rise of plastic bioelectronics," *Nature*, vol. 540, no. 7633, pp. 379–385, Dec. 2016.
[12] H. Sirringhaus, "25th anniversary article: Organic field-effect transistors: The path beyond amorphous silicon," *Adv. Mater.*, vol. 26, no. 9, pp. 1319–1335, Mar. 2014.
[13] Z. A. Lamport, H. F. Haneef, S. Anand, M. Waldrip, and O. D. Jurchescu, "Tutorial: Organic field-effect transistors: Materials, structure and operation," *J. Appl. Phys.*, vol. 124, no. 7, Aug. 2018, Art. no. 071101.
[14] A. F. Paterson *et al.*, "Recent progress in high-mobility organic transistors: A reality check," *Adv. Mater.*, vol. 30, no. 36, Sep. 2018, Art. no. 1801079.
[15] X. Jia, C. Fuentes-Hernandez, C. Y. Wang, Y. Park, and B. Kippelen, "Stable organic thin-film transistors," *Sci. Adv.*, vol. 4, no. 1, Jan. 2018, Art. no. eaao1705.
[16] T. A. Fjeldly, T. Ytterdal, and M. Shur, *Introduction to Device Modeling and Circuit Simulation*. New York, NY, USA: Wiley, 1998.
[17] G. S. Gildenblat, *Compact Modeling: Principles, Techniques and Applications*. Dordrecht, The Netherlands: Springer, 2010.
[18] C. C. McAndrew *et al.*, "Best practices for compact modeling in Verilog-A," *IEEE J. Electron Devices Soc.*, vol. 3, no. 5, pp. 383–396, Sep. 2015.
[19] A. Facchetti, "Semiconductors for organic transistors," *Mater. Today*, vol. 10, no. 3, pp. 28–37, Mar. 2007.
[20] J. E. Anthony, "The larger acenes: Versatile organic semiconductors," *Angew. Chem. Int. Ed.*, vol. 47, no. 3, pp. 452–483, Jan. 2008.
[21] J. E. Anthony, A. Facchetti, M. Heeney, S. R. Marder, and X. Zhan, "n-type organic semiconductors in organic electronics," *Adv. Mater.*, vol. 22, no. 34, pp. 3876–3892, Sep. 2010.
[22] K. Takimiya, S. Shinamura, I. Osaka, and E. Miyazaki, "Thienoacene-based organic semiconductors," *Adv. Mater.*, vol. 23, no. 38, pp. 4347–4370, Oct. 2011.
[23] A. A. Virkar, S. Mannsfeld, Z. Bao, and N. Stingelin, "Organic semiconductor growth and morphology considerations for organic thin-film transistors," *Adv. Mater.*, vol. 22, no. 34, pp. 3857–3875, Sep. 2010.
[24] C.-H. Kim *et al.*, "Decoupling the effects of self-assembled monolayers on gold, silver, and copper organic transistor contacts," *Adv. Mater. Interfaces*, vol. 2, no. 2, Jan. 2015, Art. no. 1400384.
[25] B. Kang, W. H. Lee, and K. Cho, "Recent advances in organic transistor printing processes," *ACS Appl. Mater. Interfaces*, vol. 5, no. 7, pp. 2302–2315, Apr. 2013.
[26] H. Matsui, Y. Takeda, and S. Tokito, "Flexible and printed organic transistors: From materials to integrated circuits," *Org. Electron.*, vol. 75, Dec. 2019, Art. no. 105432.
[27] K. Willa, R. Häusermann, T. Mathis, A. Facchetti, Z. Chen, and B. Batlogg, "From organic single crystals to solution processed thin-films: Charge transport and trapping with varying degree of order," *J. Appl. Phys.*, vol. 113, no. 13, Apr. 2013, Art. no. 133707.
[28] C.-H. Kim, O. Yaghmazadeh, D. Tondelier, Y. Bin Jeong, Y. Bonnassieux, and G. Horowitz, "Capacitive behavior of pentacene-based diodes: Quasistatic dielectric constant and dielectric strength," *J. Appl. Phys.*, vol. 109, no. 8, Apr. 2011, Art. no. 083710.
[29] C.-H. Kim, O. Yaghmazadeh, Y. Bonnassieux, and G. Horowitz, "Modeling the low-voltage regime of organic diodes: Origin of the ideality factor," *J. Appl. Phys.*, vol. 110, no. 9, Nov. 2011, Art. no. 093722.
[30] C.-H. Kim, Y. Bonnassieux, and G. Horowitz, "Charge distribution and contact resistance model for coplanar organic field-effect transistors," *IEEE Trans. Electron Devices*, vol. 60, no. 1, pp. 280–287, Jan. 2013.
[31] C.-H. Kim *et al.*, "A compact model for organic field-effect transistors with improved output asymptotic behaviors," *IEEE Trans. Electron Devices*, vol. 60, no. 3, pp. 1136–1141, Mar. 2013.
[32] S. Jung, J. W. Jin, V. Mosser, Y. Bonnassieux, and G. Horowitz, "A compact model and parameter extraction method for a staggered OFET with power-law contact resistance and mobility," *IEEE Trans. Electron Devices*, vol. 66, no. 11, pp. 4894–4900, Nov. 2019.
[33] S. Jung, C.-H. Kim, Y. Bonnassieux, and G. Horowitz, "Fundamental insights into the threshold characteristics of organic field-effect transistors," *J. Phys. D, Appl. Phys.*, vol. 48, no. 3, Jan. 2015, Art. no. 035106.

[34] M. Estrada, I. Mejìa, A. Cerdeira, J. Pallares, L. F. Marsal, and B. Iñiguez, "Mobility model for compact device modeling of OTFTs made with different materials," *Solid-State Electron.*, vol. 52, no. 5, pp. 787–794, May 2008.
[35] J. Zhao *et al.*, "Universal compact model for thin-film transistors and circuit simulation for low-cost flexible large area electronics," *IEEE Trans. Electron Devices*, vol. 64, no. 5, pp. 2030–2037, May 2017.
[36] J. Fan, J. Zhao, and X. Guo, "DC compact model for subthreshold operated organic field-effect transistors," *IEEE Electron Device Lett.*, vol. 39, no. 8, pp. 1191–1194, Aug. 2018.
[37] A. Castro-Carranza *et al.*, "Organic thin-film transistor bias-dependent capacitance compact model in accumulation regime," *IET Circuits Devices Syst.*, vol. 6, no. 2, pp. 130–135, Mar. 2012.
[38] O. Marinov, M. J. Deen, U. Zschieschang, and H. Klauk, "Organic thin-film transistors: Part I—Compact DC modeling," *IEEE Trans. Electron Devices*, vol. 56, no. 12, pp. 2952–2961, Dec. 2009.
[39] S. Elsaegh, U. Zschieschang, J. W. Borchert, H. Klauk, H. Zappe, and Y. Manoli, "Compact DC modeling of organic thin-film transistors including their parasitic non-linear contact effects based on a novel extraction method," *IEEE Trans. Electron Devices*, vol. 66, no. 11, pp. 4907–4914, Nov. 2019.
[40] L. Colalongo, "SQM-OTFT: A compact model of organic thin-film transistors based on the symmetric quadrature of the accumulation charge considering both deep and tail states," *Org. Electron.*, vol. 32, pp. 70–77, May 2016.
[41] F. Hain, M. Graef, B. Iñíguez, and A. Kloes, "Charge based, continuous compact model for the channel current in organic thin-film transistors for all regions of operation," *Solid-State Electron.*, vol. 133, pp. 17–24, Jul. 2017.
[42] J. Pruefer, B. Iñiguez, H. Klauk, and A. Kloes, "Compact modeling of non-linear contact resistance in staggered and coplanar organic thin-film transistors," in *Proc. Int. Conf. Org. Electron. (ICOE)*, Grenoble, France, 2018.
[43] Y. P. Tsividis and K. Suyama, "MOSFET modeling for analog circuit CAD: Problems and prospects," *IEEE J. Solid-State Circuits*, vol. 29, no. 3, pp. 210–216, Mar. 1994.
[44] O. Marinov and M. J. Deen, "Quasistatic compact modelling of organic thin-film transistors," *Org. Electron.*, vol. 14, no. 1, pp. 295–311, Jan. 2013.
[45] A. Castro-Carranza *et al.*, "Compact capacitance model for OTFTs at low and medium frequencies," *IEEE Trans. Electron Devices*, vol. 61, no. 2, pp. 638–642, Feb. 2014.
[46] H. Cortes-Ordonez, S. Jacob, F. Mohamed, G. Ghibaudo, and B. Iniguez, "Analysis and compact modeling of gate capacitance in organic thin-film transistors," *IEEE Trans. Electron Devices*, vol. 66, no. 5, pp. 2370–2374, May 2019.
[47] M. Fadlallah, W. Benzarti, G. Billiot, W. Eccleston, and D. Barclay, "Modeling and characterization of organic thin film transistors for circuit design," *J. Appl. Phys.*, vol. 99, no. 10, May 2006, Art. no. 104504.
[48] L. Li, H. Marien, J. Genoe, M. Steyaert, and P. Heremans, "Compact model for organic thin-film transistor," *IEEE Electron Device Lett.*, vol. 31, no. 3, pp. 210–212, Mar. 2010.
[49] M. Estrada *et al.*, "Frequency and voltage dependence of the capacitance of MIS structures fabricated with polymeric materials," *IEEE Trans. Electron Devices*, vol. 60, no. 6, pp. 2057–2063, Jun. 2013.
[50] J. Leise, J. Pruefer, G. Darbandy, and A. Kloes, "Charge-based compact modeling of capacitances in staggered OTFTs," in *Proc. Latin Amer. Electron Devices Conf. (LAEDC)*, Armenia, Colombia, 2019, pp. 1–4.
[51] J. Leise *et al.*, "Charge-based compact modeling of capacitances in staggered multi-finger OTFTs," *IEEE J. Electron Devices Soc.*, vol. 8, pp. 396–406, 2020.
[52] G. Horowitz, M. E. Hajlaoui, and R. Hajlaoui, "Temperature and gate voltage dependence of hole mobility in polycrystalline oligothiophene thin film transistors," *J. Appl. Phys.*, vol. 87, no. 9, pp. 4456–4463, May 2000.
[53] N. Tessler and Y. Roichman, "Amorphous organic molecule/polymer diodes and transistors—Comparison between predictions based on Gaussian or exponential density of states," *Org. Electron.*, vol. 6, nos. 5–6, pp. 200–210, Dec. 2005.
[54] S. Jung, C.-H. Kim, Y. Bonnassieux, and G. Horowitz, "Injection barrier at metal/organic semiconductor junctions with a Gaussian density-of-states," *J. Phys. D, Appl. Phys.*, vol. 48, no. 39, Oct. 2015, Art. no. 395103.
[55] R. Coehoorn, W. Pasveer, P. Bobbert, and M. Michels, "Charge-carrier concentration dependence of the hopping mobility in organic materials with Gaussian disorder," *Phys. Rev. B*, vol. 72, no. 15, Oct. 2005, Art. no. 155206.
[56] M. Waldrip, O. D. Jurchescu, D. J. Gundlach, and E. G. Bittle, "Contact resistance in organic field-effect transistors: Conquering the barrier," *Adv. Func. Mater.*, vol. 30, May 2020, Art. no. 1904576.
[57] C.-H. Kim and G. Horowitz, "Toward a fully analytical contact resistance expression in organic transistors," *Materials*, vol. 12, no. 7, p. 1169, Apr. 2019.
[58] C.-H. Kim, "Theoretical frequency limit of organic field-effect transistors," *Flex. Print. Electron.*, vol. 4, no. 4, Dec. 2019, Art. no. 044005.
[59] G. Horowitz, R. Hajlaoui, and H. Bouchriha, "The concept of 'threshold voltage' in organic field-effect transistors," *Adv. Mater.*, vol. 10, no. 12, pp. 923–927. Aug. 1998.
[60] I. G. Lezama and A. F. Morpurgo, "Threshold voltage and space charge in organic transistors," *Phys. Rev. Lett.*, vol. 103, no. 6, Aug. 2009, Art. no. 066803.
[61] O. Simonetti and L. Giraudet, "Sub-threshold current in organic thin film transistors: Influence of the transistor layout," *Org. Electron.*, vol. 14, no. 3, pp. 909–914, Mar. 2013.
[62] A. Ortiz-Conde, F. J. García-Sánchez, J. Muci, A. T. Barrios, J. J. Liou, and C.-S. Ho, "Revisiting MOSFET threshold voltage extraction methods," *Microelectron. Rel.*, vol. 53, no. 1, pp. 90–104, Jan. 2013.
[63] C.-H. Kim, S. Thomas, J. H. Kim, M. Elliott, J. E. Macdonald, and M.-H. Yoon, "Potentiometric parameterization of dinaphtho[2,3-b:2',3'-f]thieno[3,2-b]thiophene field-effect transistors with a varying degree of nonidealities," *Adv. Electron. Mater.*, vol. 4, no. 7, Jul. 2018, Art. no. 1700514.
[64] S. Jung, J. Kwon, S. Tokito, G. Horowitz, Y. Bonnassieux, and S. Jung, "Compact modelling and SPICE simulation for three-dimensional, inkjet-printed organic transistors, inverters and ring oscillators," *J. Phys. D, Appl. Phys.*, vol. 52, no. 44, Oct. 2019, Art. no. 444005.
[65] J. Kwon, S. Kyung, S. Yoon, J.-J. Kim, and S. Jung, "Solution-processed vertically stacked complementary organic circuits with inkjet-printed routing," *Adv. Sci.*, vol. 3, no. 5, May 2016, Art. no. 1500439.
[66] H. Han and C.-H. Kim, "Unexpected benefits of contact resistance in 3D organic complementary inverters," *Adv. Electron. Mater.*, vol. 6, no. 1, Jan. 2020, Art. no. 1900879.